Three-dimensional (3D) Printed Dielectric Lens and Support Structure Mounted on an Open-Ended *W*-Band Waveguide

Ian Goode and Carlos E. Saavedra

Abstract – A dielectric lens and support structure is designed and fabricated using three-dimensional printing. The lens is mounted onto an open-ended WR-10 waveguide and directly radiates into free space. The lens body has a relative permittivity that is lower than the polylactic acid (PLA) used to print the lens by lowering the infill fraction of the lens in the printer slicing software (PrusaSlicer version 2.5.0). A printed dielectric feed wedge is used to improve the radiating structure's return loss, resulting in an input reflection better than –10 dB across the entirety of WR-10 band from 75 GHz to 110 GHz. The lens exhibits a measured peak gain of 19.5 dBi at 100 GHz, with a maximum gain variation of 1.3 dB from 75 GHz to 110 GHz and uniform radiation characteristics in both the $\vec{E}$ plane and $\vec{H}$ plane. The lens provides a reduction in $\vec{E}$-plane sidelobe levels (SLLs) compared with a standard gain WR-10 horn by approximately 10 dB across the band. Further reduction in the SLLs below 100 GHz is achieved by painting the base of the lens with a conductive RF shielding paint.

1. Introduction

Dielectric lenses can increase the directivity and reduce sidelobe levels (SLLs) of radiating elements to increase the sensitivity of a radio receiver. Most dielectric lenses are presently fabricated using computerized numerical control (CNC) lathes or milling machines, but a number of works have appeared in the literature in recent years reporting three-dimensional (3D) printed dielectric lenses [1–6] and other structures at microwave and millimeter-wave frequencies [7–10]. These 3D printed structures have complex geometries and can be made at significantly lower cost both in terms of the raw materials used and, more importantly, the cost of the fabrication machinery. Furthermore, additive manufacturing offers the potential of varying the relative permittivity of dielectrics by changing the fill density in the parts [1–3, 7, 11]. The two types of 3D printing technology that are of interest for the fabrication of electromagnetic dielectric structures are fused deposition modeling (FDM) and stereolithography (SLA) resin printing. Although SLA printing provides tighter dimensional tolerances, FDM has other benefits, such as lower operating and maintenance costs.

Dielectric inserts and dielectric rods have been used as an alternative to conductive machined transitions to transition from waveguide to free space [3, 12–16]. Among these works, only the *C*-band dielectric radiating structure in [3] is fabricated using 3D printing. The remaining dielectric radiators were fabricated using conventional machining methods. In broad terms, dielectric radiators are easier to fabricate, lightweight, and require lower resolution tolerancing than metallic radiators and can function with rougher surface finishes.

In this work, a lens and feed were designed to function as a dielectric waveguide and lens to act as a radiating element directly attached to an open-ended WR-10 waveguide. The lens and feed were manufactured using FDM 3D printing with polylactic acid (PLA), using variation in the infill to control the relative permittivity of the material. A tapered feed directs the signal power toward the center of the lens. The lens is printed with a low infill fraction, and, as such, it is uniformly porous, which reduces the macroscopic permittivity of the lens body and also helps reduce the PLA dielectric losses to a full-density 3D printed lens. The lens is printed with a support structure that connects the lens to the WR-10 waveguide. To further reduce the SLLs outside of the capture angle of the lens, the outside of the support cylinder was painted with a conductive RF shielding paint. The estimated PLA material cost of the lens is well below $1 per unit. Allowing for an inexpensive and lightweight method to produce a highly directive beam at the *W* band that is useful for automotive collision avoidance radars.

2. Lens and Feed Design

The PLA used for this design was D3D Natural Tough PLA, a filament without color additives. This filament is known to have a relative permittivity of $\varepsilon_r = 2.7$ [7, 17] at the *K* band and microwave frequencies, with losses increasing at higher frequencies. The dielectric properties of this filament at the *W* band are $\varepsilon_r = 2.7$ and $\tan\delta = 0.02$. This PLA was chosen for its ease of printability on an FDM printer, the lack of additives to reduce loss, and a known simulation model. Other materials, such as photoactivated resins are used

Manuscript received 22 November 2023. This work was supported, in part, by the Natural Sciences and Engineering Research Council of Canada (grant RGPIN-2022-05204). I. Goode is a recipient of the Ontario Graduate Scholarship from the Province of Ontario, Canada, the Ian M. Drum Scholarship at Queen's University, and the Natural Sciences and Engineering Research Council of Canada Postgraduate Scholarship–Doctoral program.

Ian Goode and Carlos E. Saavedra are with the Department of Electrical and Computer Engineering, Queen's University, Kingston, Ontario, Canada K7L 3N6; e-mail: ian.goode@queensu.ca, saavedra@queensu.ca.

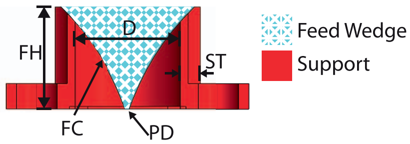

var.	FH	D	PD	ST
[mm]	8.0	8.3	0.4	1.9

Figure 1. Cross-sectional view of the feed of the lens and the support structure used to attach the lens to the WR-10 flange. Note the elliptical taper on the feed wedge denoted by FC.

in SLA printing, but these resins, although having better print tolerancing, have much higher dielectric losses.

2.1 Feed and Support Geometry

The tapered feed transition between the open-ended waveguide and lens was designed to improve the impedance match. The feed wedge protruded into the opening of the waveguide and then tapered out to the dimension of the support cylinder. This point was truncated at the level of the waveguide flange to help with manufacturability. The final design of the feed wedge is shown in Figure 1. In addition to modifying the shape of the feed to improve input matching, the dielectric constant of the feed was also engineered to improve the input match by decreasing the relative permittivity for a better match to free space. A permittivity of $\varepsilon_r = 1.67$ was selected. This lower value of relative permittivity increases the final size of the lens, but it provided a more efficient lens compared with a smaller lens with a higher infill fraction based on simulating different models of the lens. The ε_r of the PLA was lowered when printing by reducing the infill fraction of the printed part. This technique has been previously examined with added voids to the print [1, 7, 11]. The method is further simplified by using the slicer's built-in functionality to realize the lower ε_r. The relation between infill fraction and ε_r was assumed to be the relation shown in (1), where the resulting relative permittivity is equivalent to a relative permittivity that provides the same delay as the linear combination of the delay from free space and solid PLA based on the fill factor when the propagation delay is proportional to $\sqrt{\varepsilon_r}$. This is the same simplified assumption used at lower frequencies in works such as [1]. Based on this, $\varepsilon_r = 1.67$ yields a fill factor of 45%. This infill factor also reduces the loss tangent, as less of the lossy plastic will yield a loss tangent closer to that of air as expressed in (2), resulting in an approximate loss of (0.45)tan $\delta_{\text{PLA}} = 0.009$, where it was assumed that the dielectric losses were linearly proportional with fill fraction.

$$\varepsilon_r(F) = \left(F\left(\sqrt{\varepsilon_{r_{\text{PLA}}}} - 1\right) + 1\right)^2 \quad (1)$$

$$\tan\delta(F) = F\tan\delta_{\text{PLA}} \quad (2)$$

where F is the volumetric fill fraction and $\varepsilon_{r_{\text{PLA}}}$ is the relative permittivity of the PLA; in this case, $\varepsilon_{r_{\text{PLA}}} = 2.7$.

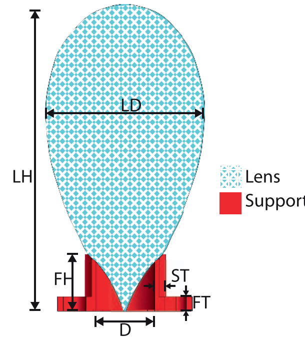

var.	FH	D	PD	ST	LH	LD
[mm]	8.0	8.3	0.4	2.0	43.2	22.4

Figure 2. Cross-sectional view of the lens and support structure.

The diameter of the feed wedge was chosen as the diameter of the mating part of the UG-387/UM flange that was used in the measurement setup. The length of the feed was designed to minimize the input reflection into the lens. The transition was further improved by using an elliptical taper to define the feed wedge, as shown by the curve FC in Figure 1. The support cylinder is a hollow structure with the same diameter as the mating flange on the WR-10 waveguide and was designed to both support the lens and to mount it to the WR-10 UG-387/UM flange. The support structure was designed as solid PLA that took advantage of the higher dielectric loss in the solid PLA to aid in attenuating any power outside of the capture area of the lens. This further helped reduce the SLLs. This surface could be metalized to reflect any power outside of the capture angle of the lens back through the support cylinder and further attenuate it. To validate this, the lens was measured with and without this metallization.

2.2 Lens Geometry

The shape of the lens was designed to equalize the phase delay from the phase center to a reference plane in space to create a directive and coherent beam. This design considered the rays as propagating from the phase center to the reference plane in a straight line and ignored any refraction at the surface of the lens, similar to linear ray assumption used at lower frequencies. These assumptions helped simplify the design process, while yielding a lens that met the desired performance goals, as shown with the experimental results in Section 3, without requiring further optimization in the simulation tool. The phase center was chosen as the center of the WR-10 waveguide at the plane of the mounting flange. The lens was radially symmetric, meaning only a single cross section of the lens needed to be designed. The contour of the lens was chosen to variably delay the propagation time through the lens to produce a plane wave at the output. This method was the same as the method derived in [1] but here for a

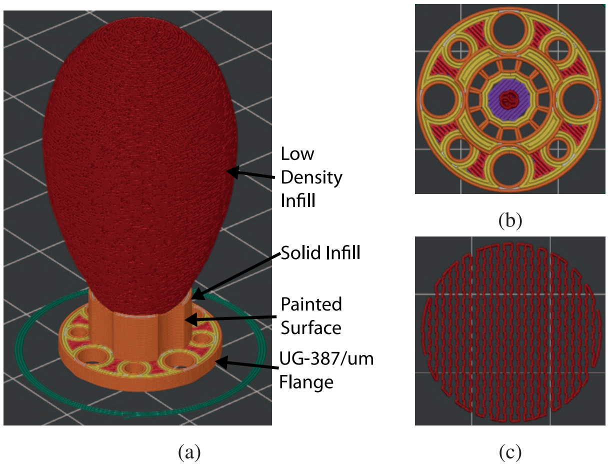

Figure 3. Sliced lens model that was used for 3D printing the two lenses. (a) Full model of the lens and support showing all layers, (b) top view showing the first few layers, including the support structure that was removed to hold the center of the feed wedge, and (c) a single layer of infill from the center of the lens showing the pattern shape.

homogenous lens on a waveguide aperture. This resulted in the lens cross section shown in Figure 2.

This lens was simulated in ANSYS HFSS Version: 2021 R1 by setting the material properties for the support material to be PLA with $\varepsilon_r = 2.7$ and tan $\delta = 0.02$ and the material properties for the lens as a reduced infill PLA with $\varepsilon_r = 1.67$ and tan $\delta = 0.009$. The cross section in Figure 2 was revolved around the center axis to produce a 3D structure. The setup was simulated twice to show the impact of the conductive paint on the support cylinder to demonstrate the SLL improvement. The paint was simulated by changing the boundary conditions on the outside of the support structure to be a finite conductive surface with a conductivity of 5.87×10^7 S/m. These simulated results are compared with the measured results in Section 3.

2.3 Fabrication

The sliced model of the lens is shown in Fig. 3. To help with printability, a single-layer feature was added for the first layer of the lens to connect the feed point to the support cylinder. This helped keep the feed point centered, as the initial contact area was small on the print platform. This first layer is visualized in Figure 3b and was manually removed after printing. The density of the PLA was selectively decreased by using the slicer's built-in infill options. A PrusaSlicer Version 2.5.0 was used to slice the lens and generate the printer control code (GCODE) from the computer-aided design model in Figure 2. The combination of the lens and support structure is shown in the slicer in Figure 3a, with separate parameters applied to each. The support cylinder was printed solidly from PLA, and the lens was entirely defined as infill using the built-in 3D honeycomb pattern, as this eliminated any continuous gaps in the infill. The infill pattern is shown for a single layer in Figure 3c. The lens was printed without external perimeters to keep the relative permittivity uniform through the lens. This lens and support structure were printed with a layer height of 0.2 mm for all layers.

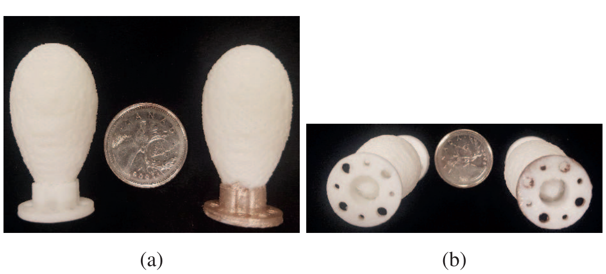

Figure 4. The FDM 3D printed lenses. (a) Side view: the left lens has a painted support structure, and the right is unpainted, (b) End view showing the feed wedge for the lenses.

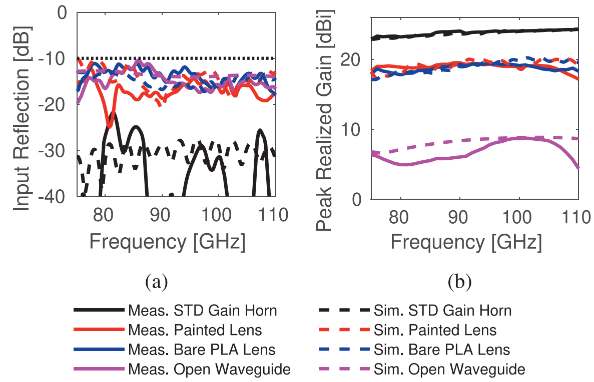

Figure 5. Measured and simulated: (a) input reflection and (b) peak realized gain.

Two identical copies of the lens were 3D printed using an FDM printer, with a material cost of less than \$1 per lens. The two printed lenses are shown in Figure 4. One of the lenses had its support base painted using MG Chemicals 843WB Super Shield conductive paint that has a rated resistivity of 5.3×10^{-4} Ω cm. Four coats of the paint were brushed onto the support cylinder. The final printed lenses had a mass of 6.03 g for the nonpainted lens and 6.11 g for the painted lens. Both are less than the mass of the 24 dBi standard gain horn (Eravant SAZ-2410-10-S1) at 38.43 g.

3. Measured Results

All measurements were performed in-house using an Anritsu MG3694A signal generator, an Eravant-SFA-753114513-10SF-E1 frequency multiplier, and an Eravant STD-10SF-NI power detector to implement a unidirectional scalar network analyzer at the W band.

The input reflection to the device under test (DUT) was found using the frequency multiplier, power meter, and an Eravant WR-10 directional coupler (SWX 75311420-10-4B). An offset short (SSL) calibration was performed to report the input reflection to each DUT. The resulting plot of input reflection is compared with the simulated input reflection (shown in Figure 5a). The

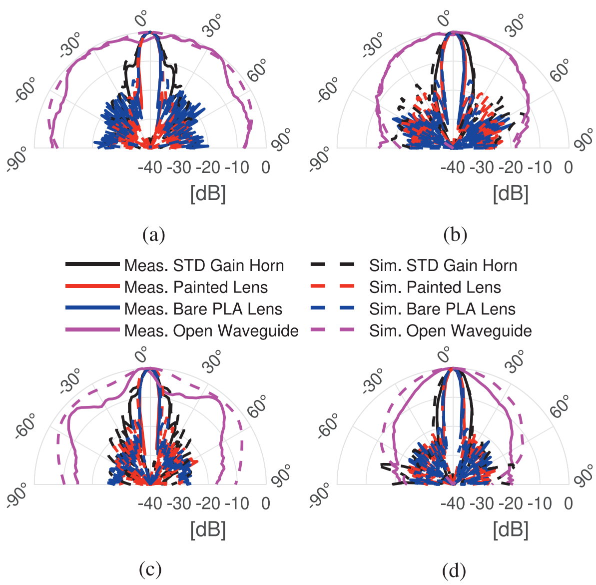

Figure 6. Normalized radiation patterns a for the $\vec{E}$-plane cut and the $\vec{H}$-plane cut: (a) 80 GHz $\vec{E}$ plane; (b) 80 GHz $\vec{H}$ plane; (c) 100 GHz $\vec{E}$ plane; and (d) 100 GHz $\vec{H}$ plane.

measured input reflection for the lens with and without the painted support had an input reflection less than –10 dB from 75 GHz to 110 GHz.

To measure the far-field characteristics of the DUT, a single-axis rotational stage was used to rotate each antenna about its phase center. To report measured antenna gain, two identical standard gain horns (Eravant SAZ-2410-10-S1) were used to calculate the path loss with the horns pointed at the boresight. Figure 5b shows a comparison of the measured and simulated peak gain for the lens with and without the painted support, compared with a standard gain (24 dBi) horn and an open-ended waveguide. The measured lens provided a peak gain of 19.5 dB at 100 GHz with a maximum gain variation of 1.3 dB. This peak gain is 10 dB more than the peak gain from the open-ended waveguide without the lens.

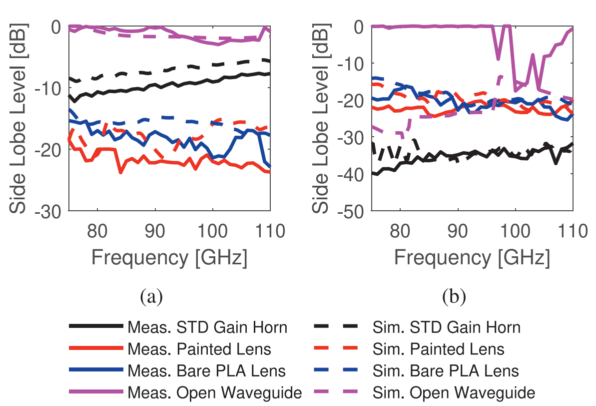

Figure 7. All measured and simulated SLLs across the band. (a) SLL in the $\vec{E}$-plane cut and (b) SLL in the $\vec{H}$-plane cut.

Table 1. Comparison table between this work and select millimeter-wave dielectric lenses comparing far-field measured results at respective midband

Reference	Lens topology	Gain (dBi)	$\vec{E}$ SLL (dB)	Bandwidth (GHz)	Construction method
This work	Homogenous	19.5	22	75–110	FDM low fill
[6]	Homogenous	18	—[a]	215–420	FDM solid
[13]	Homogenous	—[a]	10	60–65	CNC
[18]	Gradient ε_r	30	—[a]	90–100	CNC

[a] Result not given in source.

Measured normalized radiation patterns are shown at the midband in Figure 6 for the $\vec{E}$-and $\vec{H}$-plane field cuts for the painted and unpainted lens, the standard gain horn, and the open-ended waveguide. Normalized radiation patterns are shown to compare the SLLs between the lenses and the standard gain horn. The lens produces a uniform beamshape across the band in both field cuts with and without the paint.

A comparison of the SLLs for all setups are shown in Figure 7. As can be observed from the radiation patterns in Figure 6, the lenses reduce the SLLs in the $\vec{E}$ plane. The painted support base lens can be seen to further reduce the SLLs in both cuts below 100 GHz compared with the nonpainted lens. Finally, a comparison to other 3D-printed *W*-band antennas is presented in Table 1.

4. Conclusion

A FDM 3D-printed lens is presented that provides a large gain enhancement over an open-ended waveguide and can produce a more narrow and radially symmetric main beam than a standard gain waveguide horn without the need to machine metallic structures using a simple design procedure. The lens simplifies the design process by using only slicer settings to achieve the modification to the relative permittivity. The result is improved SLLs in the $\vec{E}$ plane and consistent impedance match and peak realized gain across the band. Further reduction in the SLL was shown by painting the outside of the lens's support structure with a conductive paint. In addition to the performance improvements, the lens is less expensive to fabricate and more lightweight than comparable metal parts without the need for high-tolerance machining, providing a cost-effective structure for millimeter-wave applications.

5. References

1. I. Goode and C. E. Saavedra, "3D Printed Linearly Polarized X-Band Conical Horn Antenna and Lens," *IEEE Open Journal of Antennas and Propagation*, **3**, May 2022, pp. 549-556.
2. K. V. Hoel, M. Ignatenko, S. Kristoffersen, E. Lier, and D. S. Filipovic, "3D Printed Monolithic GRIN Dielectric-Loaded Double-Ridged Horn Antennas," *IEEE Transactions on Antennas and Propagation*, **68**, 1, September 2019, pp. 533-539.

3. E.-S. Jo and D. Kim, “3D Printer Based Lens Design Method for Integrated Lens Antennas,” *IEEE Antennas and Wireless Propagation Letters*, **17**, 11, 2018, pp. 2090-2093.
4. Y.-X. Zhang, Y.-C. Jiao, and S.-B. Liu, “3D Printed Comb Mushroom-Like Dielectric Lens for Stable Gain Enhancement of Printed Log-Periodic Dipole Array,” *IEEE Antennas and Wireless Propagation Letters*, **17**, 11, November 2018, pp. 2099-2103.
5. G.-B. Wu, K. F. Chan, W. C. Mok, and C. H. Chan, “3D Printed Terahertz Lens for Bessel Beam Generation,” IEEE Asia-Pacific Microwave Conference, Singapore, Singapore, December 10–13, 2019, pp. 637-639.
6. E. Lacombe, F. Gianesello, A. Bisognin, C. Luxey, D. Titz, et al., “Low-Cost 3D-Printed 240 GHz Plastic Lens Fed by Integrated Antenna in Organic Substrate Targeting Sub-THz High Data Rate Wireless Links,” 2017 IEEE International Symposium on Antennas, San Diego, CA, USA, July 9–14, 2017, pp. 5-6.
7. I. Goode and C. E. Saavedra, “3D Printed 18 GHz to 28 GHz Horn Antenna and Gradient Index of Refraction Lens,” 2021 XXXIVth General Assembly and Scientific Symposium of the International Union of Radio Science, Rome, Italy, October 4, 2021.
8. H. Qiao, X. Lv, J. Mou, and D. Guo, “Low-Cost and Low-Profile W-Band Antenna-Coupled Detector Array,” 2019 12th UK-Europe-China Workshop on Millimeter Waves and Terahertz Technologies, London, UK, August 20–22, 2019.
9. F. Machado, P. Zagrajek, V. Ferrando, J. A. Monsoriu, and W. D. Furlan, “Multiplexing THz Vortex Beams With a Single Diffractive 3D Printed Lens,” *IEEE Transactions on Terahertz Science and Technology*, **9**, 1, January 2019, pp. 63-66.
10. T. Skaik, Y. Wang, M. Salek, P. Hunyor, H. Wang, et al., “A 3D Printed 300 GHz Waveguide Cavity Filter by Micro Laser Sintering,” *IEEE Transactions on Terahertz Science and Technology*, **12**, 3, May 2022, pp. 274-281.
11. P. Kadera, J. Lacik, and H. Arthaber, “Effective Relative Permittivity Determination of 3D Printed Artificial Dielectric Substrates Based on a Cross Unit Cell,” *Radioengineering*, **30**, 4, December 2021, pp. 595-610.
12. M. Sporer, R. Weigel, and A. Koelpin, “A 24 GHz Dual-Polarized and Robust Dielectric Rod Antenna,” *IEEE Transactions on Antennas and Propagation*, **65**, 12, December 2017, pp. 6952-6959.
13. C. Fernandes, E. B. Lima, and J. R. Costa, “Tapered Waveguide Feed for Integrated Dielectric Lens Antenna Performance Tests,” 2021 IEEE International Conference on Computer as a Tool, Lisbon, Portugal, April 27–29, 2011.
14. A. Papió-Toda, S. Amaya, L. Jofre, and F. De Flaviis, “Lens Antenna Probe for Near-Field W-Band Imaging,” IEEE International Symposium on Antennas and Propagation, Spokane, WA, USA, July 3–8, 2011, pp. 2569-2572.
15. Y. Wang, F. Qi, Z. Liu, P. Liu, W. Li, et al., “Wideband Method to Enhance the Terahertz Penetration in Human Skin Based on a 3D Printed Dielectric Rod Waveguide,” *IEEE Transactions on Terahertz Science and Technology*, **9**, 2, March 2019, pp. 155-164.
16. C. Gu and L. Bai, “Study of 140 GHz Waveguide Fed Lenses With Different Dielectric Constant,” 2021 IEEE Microwave Theory and Techniques in Wireless Communications, Riga, Latvia, October 7–8, 2021, pp. 258-262.
17. H. Banting and C. E. Saavedra, “Dielectric Spectroscopy of Fluids and Polymers for Microwave Microfluidic Circuits and Antennas,” *IEEE Transactions on Microwave Theory and Techniques*, **69**, 1, January 2021, pp. 337-343.
18. A. E. Mahmoud, W. Hong, Y. Zhang and A. Kishk, “W-Band Multilayer Perforated Dielectric Substrate Lens,” *IEEE Antennas and Wireless Propagation Letters*, **13**, April 2014, pp.734-737.